

Electronic Supplementary Information

High and Reversible Oxygen Uptake in Carbon Dot Solutions Generated from Polyethylene Facilitating Reactant-Enhanced Solar Light Harvesting

Sanjit Mondal, ^{†1}Pitchiah E Karthik, ^{†1}Lipipuspa Sahoo, ¹Kaustav Chatterjee, ^{1}M. Sathish² and Ujjal K. Gautam^{*1}*

¹*Department of Chemical Sciences, Indian Institute of Science Education and Research (IISER)-Mohali, Sector 81, Mohali, SAS Nagar, Punjab 140306, India*

²*Functional Materials Division, CSIR-Central Electrochemical Research Institute, Karaikudi 630 003, India*

**Corresponding author: ujjalgautam@iisermohali.ac.in, ujjalgautam@gmail.com*

([‡]Current address: Department of Chemistry, Indiana University, Bloomington, IN 47405 (USA))

([†]These authors contributed equally)

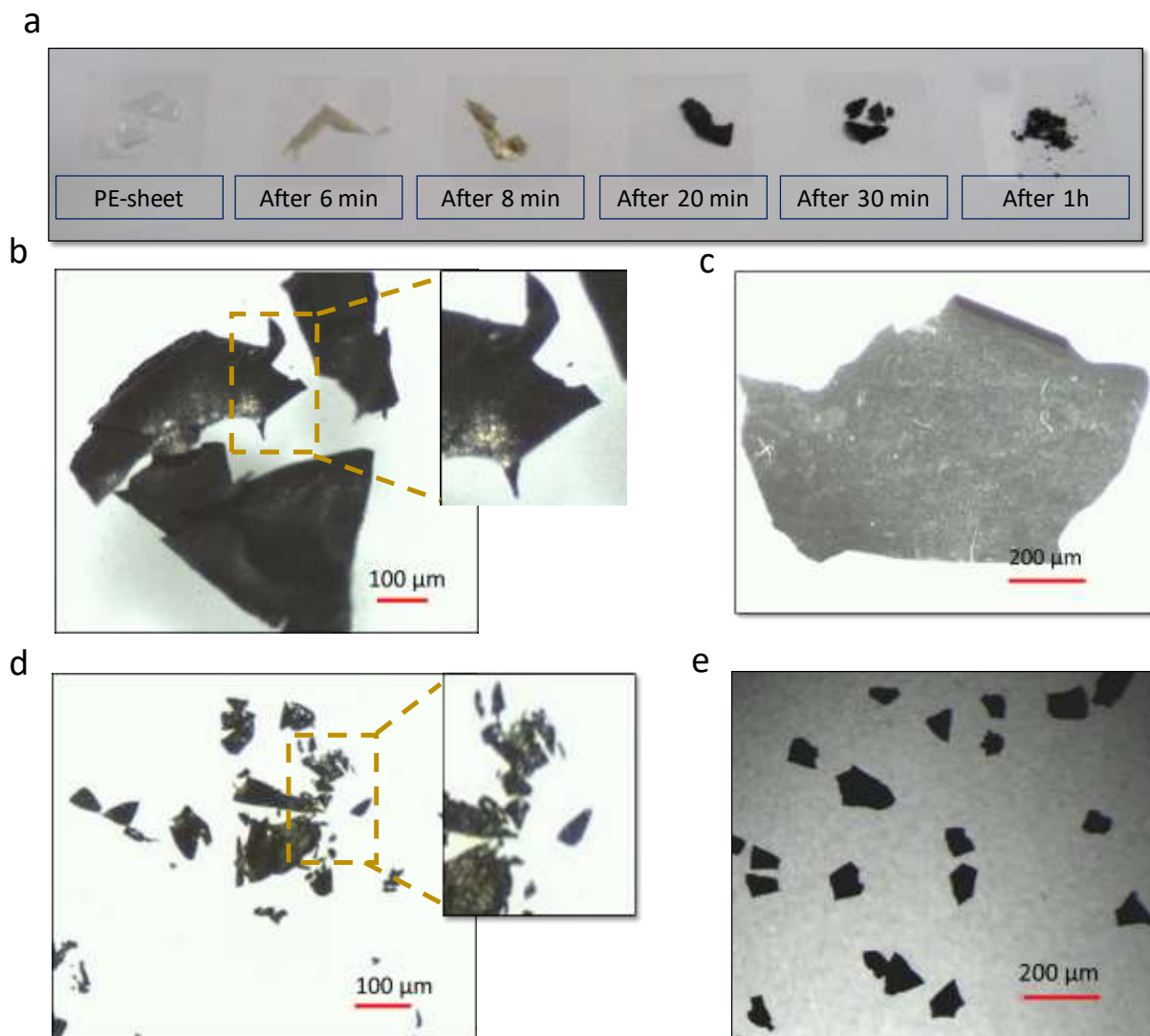


Fig. S1. (a) Photographs showing typical changes in the appearance of PE during acid treatment under reflux conditions. The PE pieces lose their transparency within six minutes, accompanied by evolution of a Raman band corresponding to graphene as discussed in main text. The PE pieces also get curled gradually. The pieces appear black within 20 min. However, they remain elastic until 30 min. The pieces become crisp after 60 min and can be easily crushed by pressing. The smaller sizes obtained after 60 minutes is probably due to stirring induced shear pressure. (b, c) Optical microscopy images of two such small pieces. Inset in b shows a piece with sharp edges suggesting inhomogeneity in charring within the sheet. (d, e), The charred mass after KMnO_4 treatment becomes much smaller, forming a homogeneous dispersion in the reaction medium.

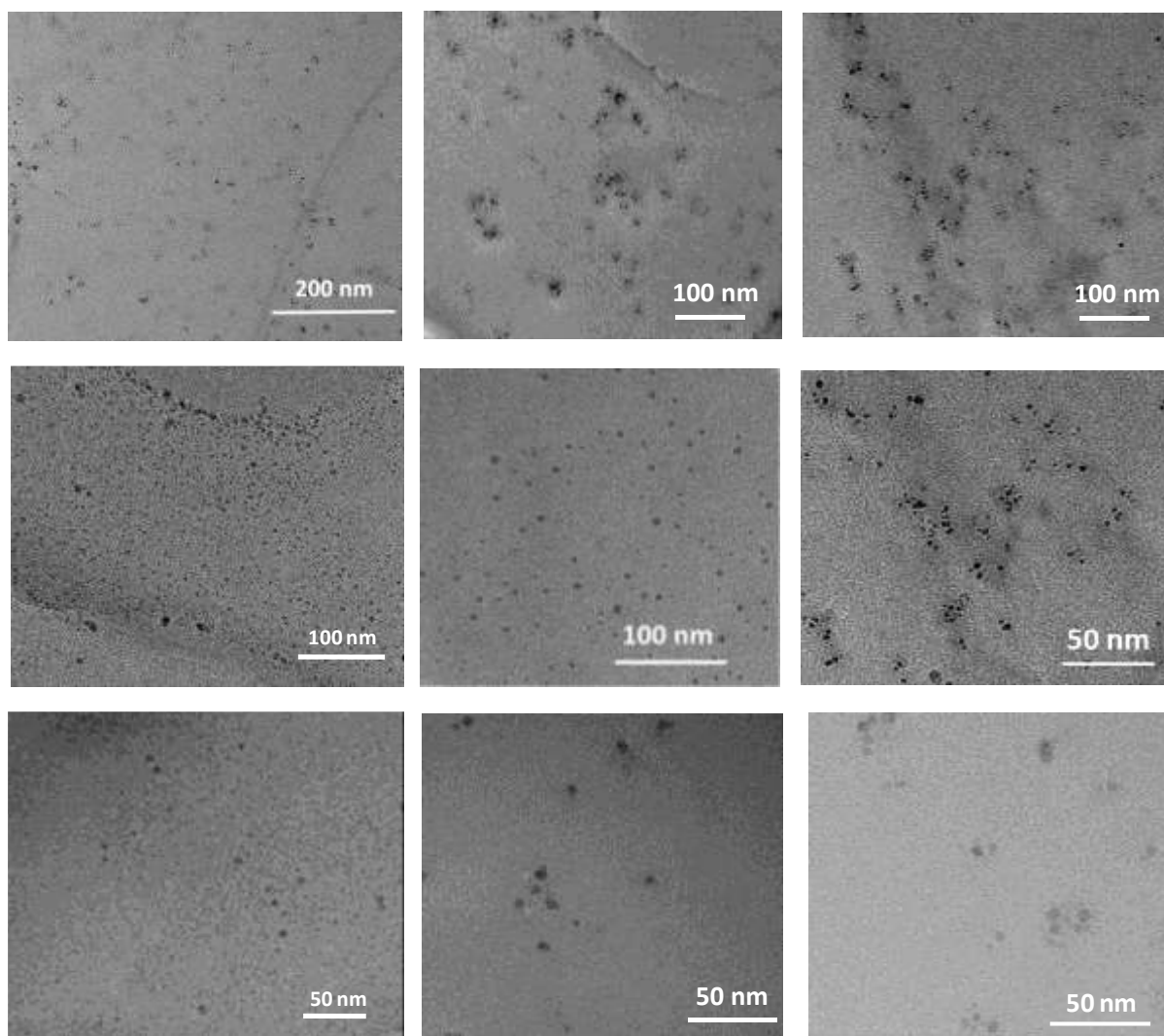


Fig. S2. TEM images of PE-CQDs at different magnifications. Most of the particles are sub-10 nm in size. However, few particles are bigger and non-spherical in nature.

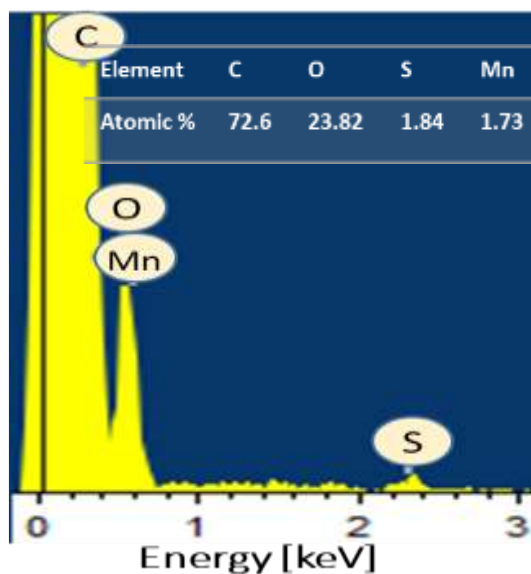


Fig. S3. EDS spectrum of the PE-sample after treatment with KMnO_4 shows the presence of C, O, S and Mn (the carbon tape on which the sample was loaded might have contributed to the C and O signal). The atomic ratio of the S and Mn is 52:48. No Mn was however detected in the purified PE-CQDs after H_2O_2 treatment as discussed in Figure S4.

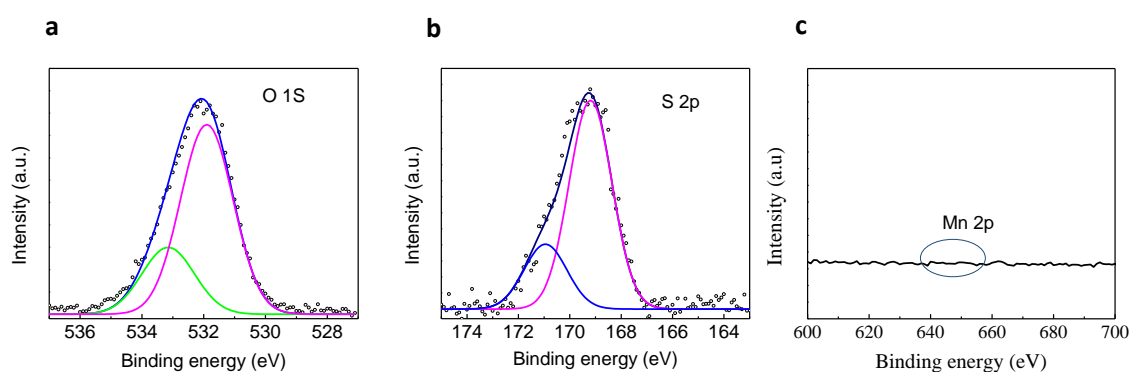
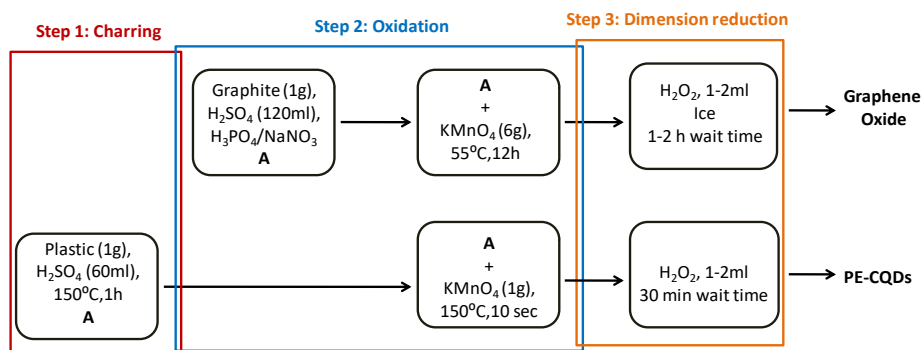


Fig. S4. XPS spectrum recorded on the PE-CQDs corresponding to O 1s (a) and S 2p (b). (c) In order to ensure the absence of any Mn impurity which might get incorporated into the CQDs during oxidation by KMnO_4 , we recorded the XPS spectrum in the Mn region. No Mn signal was detected.



The PE-CQD fabrication method has some similarities and at the same time, certain key differences with the Hummer's method as seen from the following discussion. In fact, we show below that Hummer's method using graphite as precursor cannot be extended for CQD synthesis. The main differences are: 1) PE-CQD method can be loosely considered as three step method: Step 1 is acid charring, step 2 is oxidation of the char, step 3 is the creation of 0D CQDs from the oxidized char. Thus CQD method has an extra step of dehydrogenation and charring.

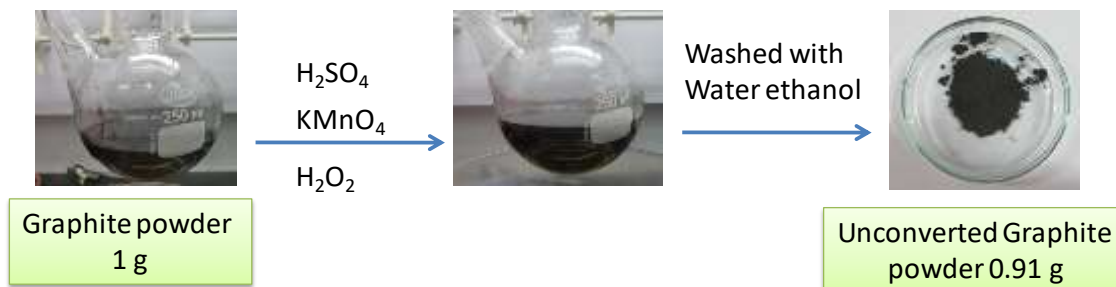


Fig. S5: Synthesis of CQDs using graphite powder as precursor. Barely any CQD was found after the reaction. Black powder was collected at the end of the reaction.

From the view point of reduction in dimensionality: Hummer's method is 3D→2D conversion involving only Vander Waals bonds rupture while PE-CQD method is 3D→0D conversion involving both covalent & Vander Waals bond rupture. 3) Graphite as a precursor does not work in PE-CQD method and this is a vital difference between with Hummer's methods. To demonstrate the same we carried out the PE-CQD synthesis with graphite powder as a starting material. We kept the other reaction condition same. This did not result in any visible colour change, which confirms that CQDs formation did not occur appreciably. We have centrifuged the whole solution and washed with water followed by ethanol, dried at 90 °C and collected the unconverted graphite powder. Out of 1 g of graphite powder used, 0.91 g graphite powder was left-over as shown in Figure S5.

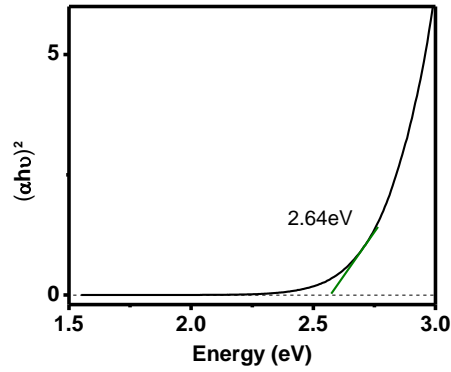


Fig. S6: Optical band gap calculation of PE-CQDs using the Tauc plot.

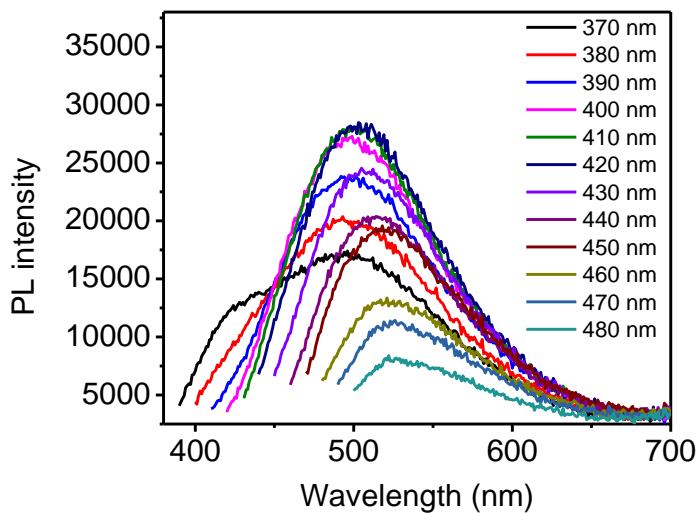


Fig. S7: Emission spectra of PE-CQDs under different excitation wavelengths (from 360 to 480 nm).

We have recorded PL spectra with different excitation wavelengths (370-480 nm) and a red-shift of maximum emission wavelength was observed as the excitation wavelength was red-shifted. The emission intensity increased with the shifting of excitation wavelength from 270 to 420 nm, while a decrease in intensity was observed beyond 420 nm (430-480 nm) as shown in below. The maximum fluorescence intensity was observed at 500 nm, when using an excitation wavelength of 420 nm.

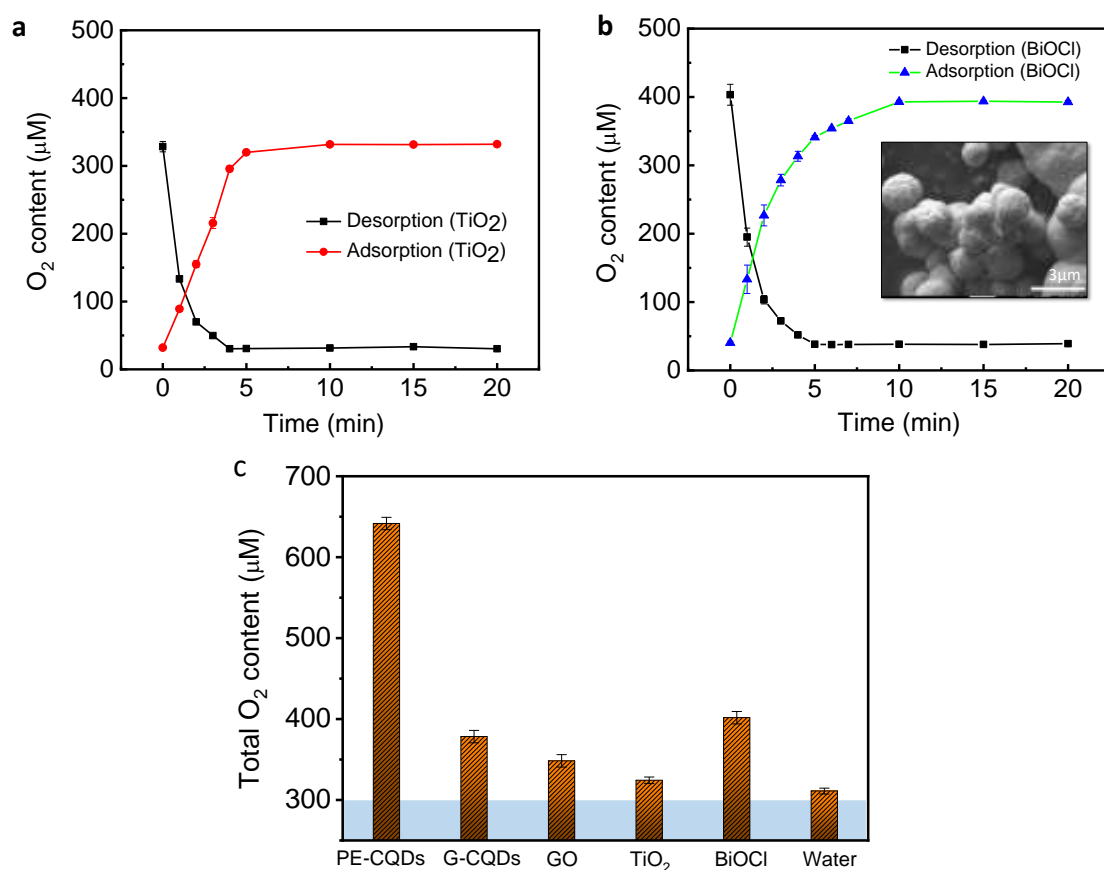


Fig. S8: Temporal variation of total oxygen content in (a) TiO₂ and (b), BiOCl aqueous solution during purging with nitrogen and subsequently during spontaneous oxygen uptake from air by the nitrogen saturated solutions. (c) Total O₂ content measurement of G-CQDs, GO, TiO₂ and BiOCl materials.

Oxygen content in aqueous dispersions of different photocatalysts: Estimation of total oxygen content (TOC) in photocatalyst containing aqueous aliquots have shown that the TOC level indeed dependent on the suspended material. To compare the effect of PE-CQDs, we have estimated changes in the TOC levels under identical conditions using aqueous suspension of 25 mg each of commercial (P-25) TiO₂ (Fig. S8a) and BiOCl (Fig. S8b), (XRD pure BiOCl was prepared by a reported hydrothermal method.¹ SEM image (as in inset of Fig. S8b) shows that these micrometer-size particles are spherical in shape.) The plots show that saturated O₂ level is ~325 μM in TiO₂, close to the value for pure water, while the same is marginally higher (410 μM) in the case of BiOCl (measurements of oxygen content were carried out 0.5 mm below the aqueous surface having 20 cm² surface area). Fig. S8c is the total O₂ content measurement of Glucose derived CQD (G-CQDs), GO, TiO₂ and BiOCl materials together.

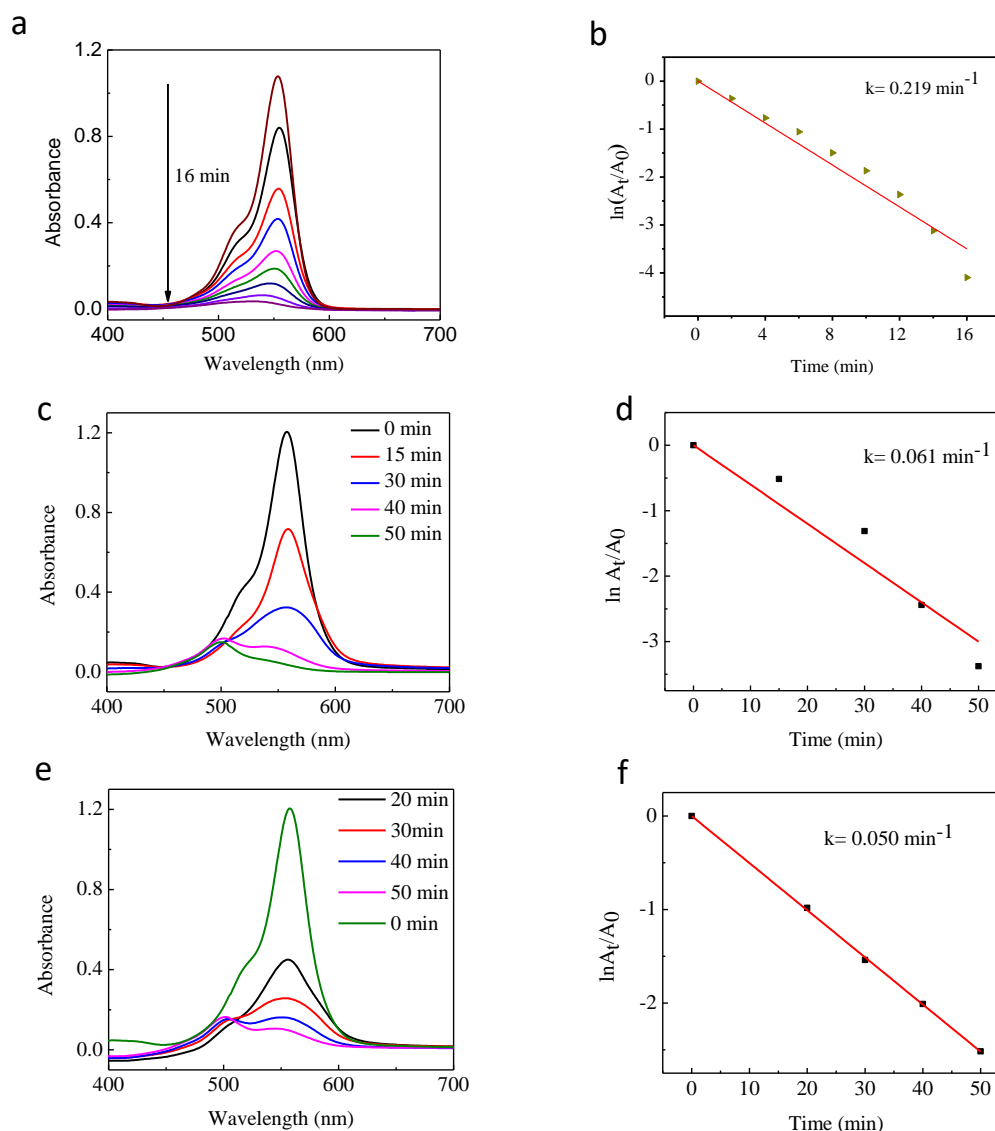


Fig. S9. UV-visible absorption spectra of Rh-B at different time interval during catalytic degradation using PE-CQDs for the 1st cycle (a), Plot of $\ln(A_t/A_0)$ vs. time of Rh-B photo-degradation for the 1st cycle (b). UV-visible absorption spectra of Rh-B at different time interval during catalytic degradation using PE-CQDs after 40th cycle (c), Plot of $\ln(A_t/A_0)$ vs. time of Rh-B photo-degradation after 40th cycle (d). UV-visible absorption spectra of Rh-B at different time interval during catalytic degradation using PE-CQDs after 100th cycle (e), Plot of $\ln(A_t/A_0)$ vs. time of Rh-B photodegradation after 100th cycle (f).

Photocatalytic performance of PE-CQDs: Photocatalytic degradation reactions were performed in a 100 mL glass beaker using a 400 W Xe lamp (Newport, USA) attached with an IR filter. 10 mg of PE-CQD was added to a 25 ml solution of 12 μ M RhB and kept in dark for 30 min to ensure an adsorption/desorption equilibrium of the dye on catalyst surface and then the resulting aliquot was

exposed to light. The degradation efficiencies of RhB were evaluated using the UV-Visible absorption spectroscopy and monitoring the absorption peak at 553 nm. The kinetics of the reaction was monitored by taking out 1 ml of solution from the reaction cell at regular intervals of time and analysing it based on Beer-Lambert law. We have calculated degradation efficiency (η) by using the following equation:

$$\eta = [1 - (A_t/A_o)] \times 100\%$$

where A_o = initial absorbance and A_t = absorbance of dye solution at reaction time t . We have also carried out stability and recyclability test for the PE-CQDs for 100 cycles in the following manner: Once the first cycle of degradation was over, 10 μ L of 10 M stock solution of RhB was added to the same reaction mixture (which ensures that the absorption intensity at 553 nm becomes almost same as that at the beginning of the first cycle). This process was continued for 100 cycles without any intermittent cleaning of the PE-CQDs.

Assessment of photocatalytic properties of PE-CQDs: The photocatalytic activity and recyclability of the PE-CQDs were found to be remarkable in comparison to many other efficient photocatalysts reported till date, when investigated for the degradation of Rhodamine-B(RhB) dye, a notable color pollutant. Fig. S9 shows the temporal evolution of UV-Visible absorption spectra of the RhB solution exposed to light in presence of PE-CQDs 1st cycle, after 40th and 100th cycle.

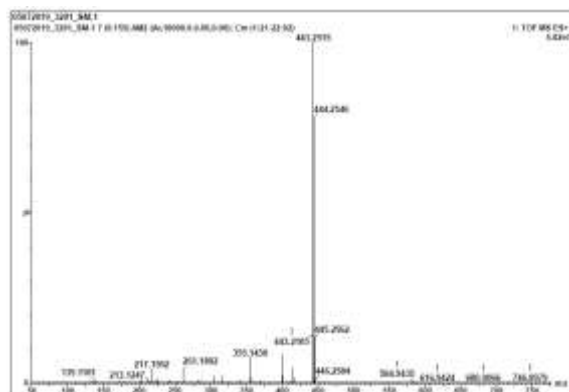
The temporal UV-visible spectral changes of RhB aqueous solution during its photo-degradation using PE-CQD is shown in Fig. S9a. The absorption corresponding to the λ_{max} for RhB at 553 nm gradually decreased exhibiting a reaction rate-constant of 0.22 min^{-1} and turnover frequency of 22.01 $\text{min}^{-1}\text{g}^{-1}$ (Fig. S9b). As seen in these plots, the variation in these cycles are not extensive. The rate constant and TOF for the reaction after 100 cycle is 0.05 min^{-1} and 5.0 $\text{min}^{-1}\text{g}^{-1}$ respectively, which is comparable to efficiencies of fresh and efficient photocatalysts such as nanocrystalline TiO_2 , $\text{g-C}_3\text{N}_4$ and Ag/AgFeO_2 exhibiting rate constants 0.0654 min^{-1} , 0.0243 min^{-1} , 0.040 min^{-1} respectively and TOF of 2.6 $\text{min}^{-1}\text{g}^{-1}$, 0.81 $\text{min}^{-1}\text{g}^{-1}$ and 1.6 $\text{min}^{-1}\text{g}^{-1}$ respectively as shown in Table S2. We have further carried out RhB degradation with commercial P-25 under identical conditions (i.e. weight of the catalyst, dye concentration, light intensity since there is considerable variation in reaction conditions in most literature reports). The rate constant and TOF values for P-25 were found to be 0.0956 $\text{min}^{-1}\text{g}^{-1}$ and 9.5 $\text{min}^{-1}\text{g}^{-1}$.

Comparison of RhB degradation products by PE-CQDs and benchmark commercial TiO₂,

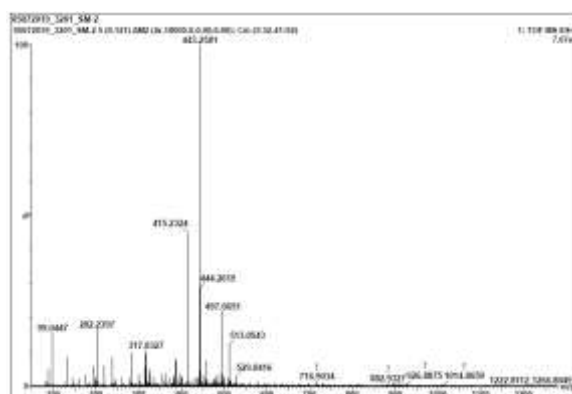
HRMS study: We have carried out additional HRMS studies to establish degradation of Rhodamine B dye. It was found that the RhB indeed degraded completely after irradiation of light for 16 min. To examine this, we have taken out samples at different time interval during RhB photo-degradation and recorded HRMS spectra to measure how much RhB has degraded and what is the nature of the degraded product. The HRMS spectra of the Rh-B at 0 min, 8 min and 16 min are given below (Fig. S10a). It was observed from the HRMS data that the $m/z = 443$ corresponding to RhB completely disappeared after light irradiation for 16 min. The spectrum recorded after 8 min of reaction shows the appearance of many new, reasonably-intense peaks with lower molecular mass ($m/z=415$ corresponds single de-ethylated RhB, and even lower $m/z= 202, 99$ etc. corresponding to various smaller fragments). Besides, at 16 min, it is to be pointed out that m/z peaks with lower values have increased.

We compared our findings with commercial TiO₂ (P-25), a widely studied benchmark photocatalyst for RhB degradation. Note that the degradation using the PE-CQDs is twice as fast as that of P-25 under identical conditions. We have recorded HRMS spectra of RhB degradation solution after complete degradation (33 min) and half-way the reaction (16 min) (Fig. S10b). The results are comparable. TiO₂ also shows a peak at m/z of 415 indicating deethylation as one of the degradation mechanisms. Besides, the peak at $m/z = 99$ is the most intense peak in both the degradation processes.

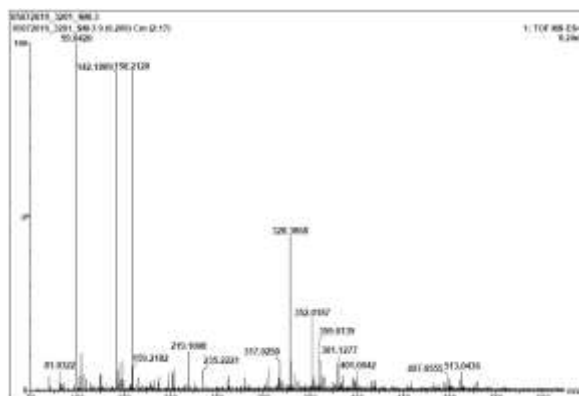
Thus the HRMS data establish the nature of degradation in PE-CQDs and benchmark P-25 TiO₂ catalyst is similar and the changes in the UV-Vis spectra are not due to decolorization.



time=0 min

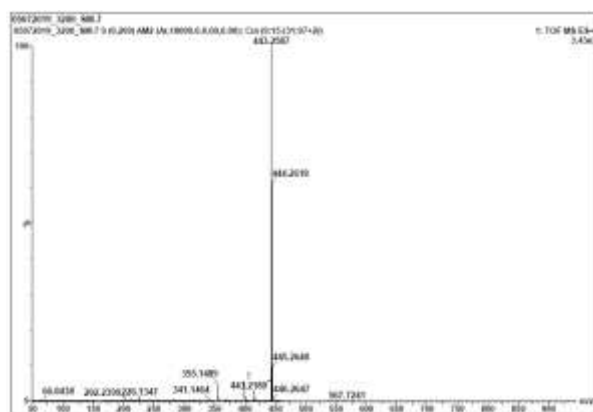


time=8 min ($t_{1/2}$)

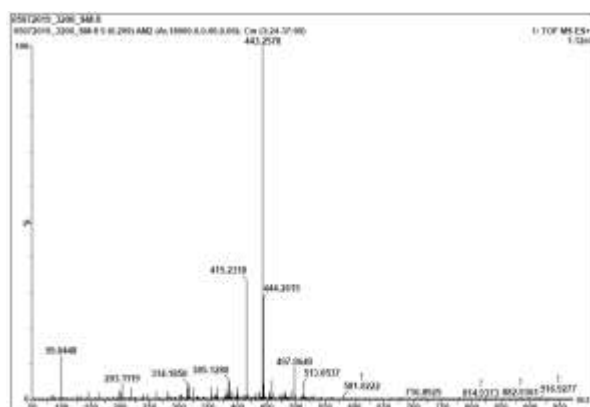


time=16 min (t_{final})

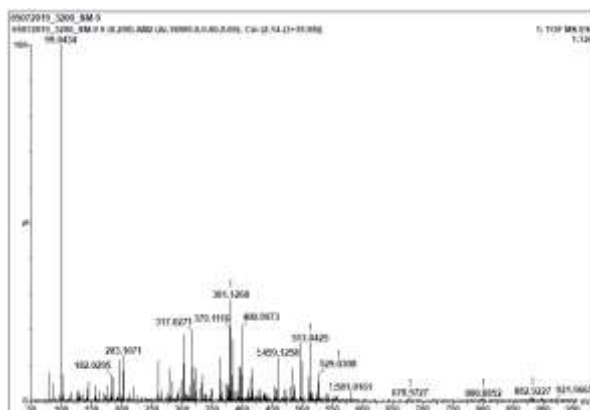
Fig. S10a: HRMS spectra of the photo-degradation reaction mixture of RhB and PE-CQDs at different time intervals: (a) 0 min, (b) 8 min and (c) 16 min.



time=0 min



time=16 min ($t_{1/2}$)



time=33 min (t_{final})

Fig. S10b: HRMS spectra of the photo-degradation reaction mixture of RhB and TiO₂ at different time intervals: (a) 0 min, (b) 16 min and (c) 33 min

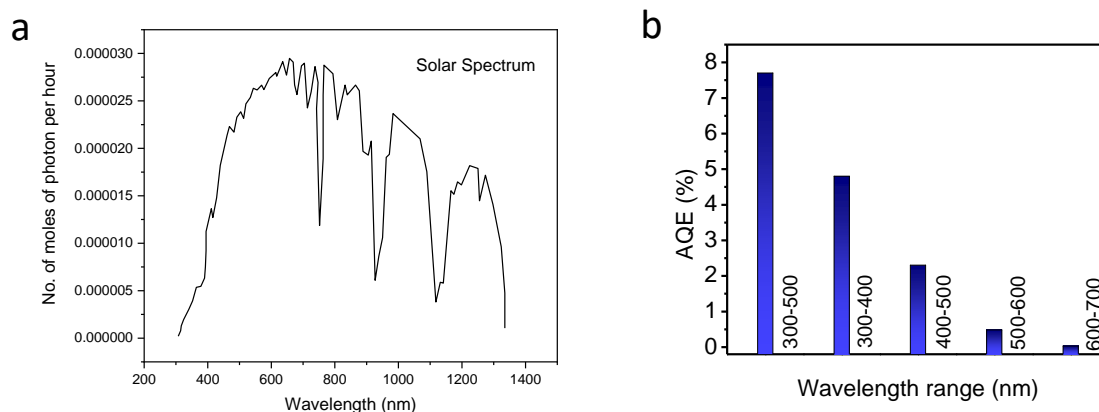


Fig. S11: a, Solar spectrum. b, The AQE (%) in different wavelength regions for the photocatalytic benzyl alcohol oxidation (detailed in Note S1).

Origin of activity: We have carried out 2 sets of experiments to demonstrate that high O_2 content can indeed improve the reaction rate. Set 1 is based on CH_3CN solvent and Set 2 is based on water as solvent (since O_2 measurements were carried out in water only).

Set 1: Herein we have used 4 reactions with different amounts of O_2 content in CH_3CN and Water separately. The first one is by purging oxygen gas during reaction, as is usually done in other investigations from literature. The second was in air where O_2 enrichment occurred only because of PE-CQDs. In third attempt, we thoroughly purged N_2 in CH_3CN and then added PE-CQD to it (here CQDs are already saturated with O_2). In the fourth approach, we passed N_2 in the PE-CQD solution to expel maximum possible dissolved O_2 . We expected, based on observations in water, that there should not be much difference in reaction yield between the first and the second reaction. Between the third and the fourth approach, 3rd should provide better yield since we added PE-CQDs saturated with O_2 which would lead to more O_2 content. On the contrary, the 4th approach will drive away oxygen from the PE-CQDs as well as from solvent. We observed that the reaction yields varied accordingly, as given in the following Fig. S12a.

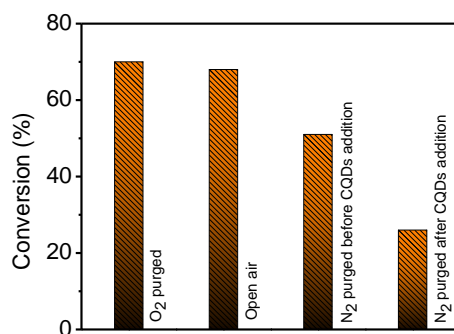


Fig. S12a: Relative conversion efficiency of PE-CQDs in CH₃CN under different oxygenated conditions confirming that the higher oxygen solubility can improve the photocatalytic oxidation efficiency.

Set 2: To ascertain the role of oxygen present on the CQDs we have performed the reaction in water medium (a poor medium due to poor solubility of reactants) and the results are shown below. For the sake of easy comparison, the maximum yields were considered as 100% yields. The actual yields in CH₃CN solvents were 70%, 68%, 51% and 26%. The yields in water were 23%, 21%, 15% and 6% for oxygen contents of >1000 μM, 640 μM, 320 μM and 95 μM respectively (NOTE: >1000μM and 640 μM is not expected to make much difference as in both cases, the CQD surface would be saturated, and the difference is only due to the oxygen dissolved in water, which is inconsequential). The data shows that the yield of the reaction is certainly dependent on the oxygen content in the solution. The results of SET 1 and SET 2 are compared in Fig. S12b (for easy comparison, the maximum yields were considered as 100% yields)

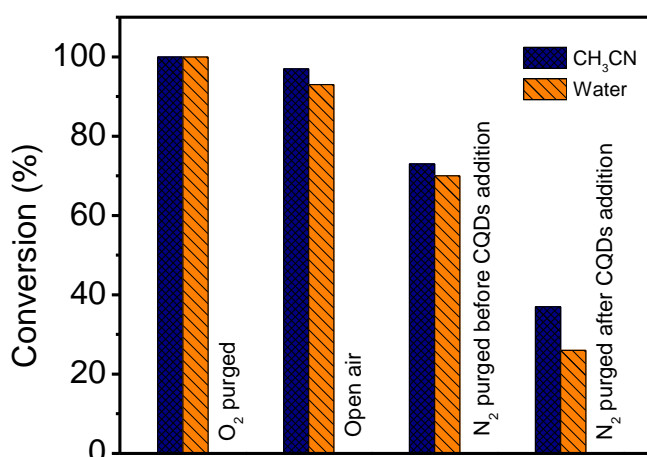


Fig. S12b: Relative conversion efficiency of PE-CQDs in CH₃CN and in water under different oxygenated conditions demonstrating that the O₂ contents correspond to conversion efficiency.

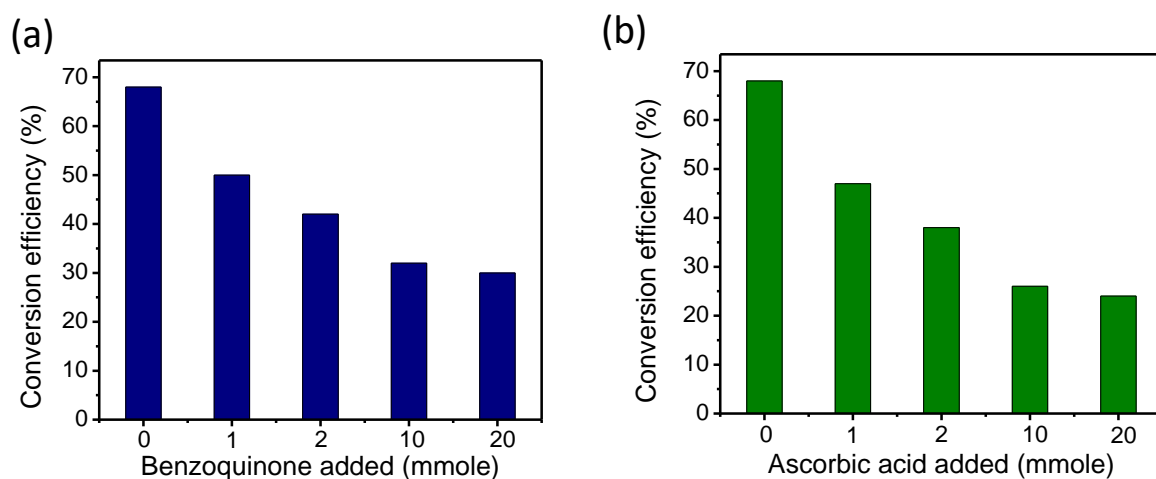


Fig. S13: The BA conversion efficiency in addition of different amount of superoxide radical anion scavenger (a) benzoquinone and (b) ascorbic acid.

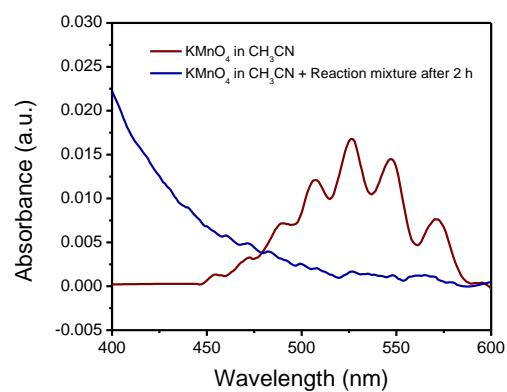


Fig. S14: The UV-Visible spectra recorded before and after addition of reaction aliquot in the KMnO_4 solution.

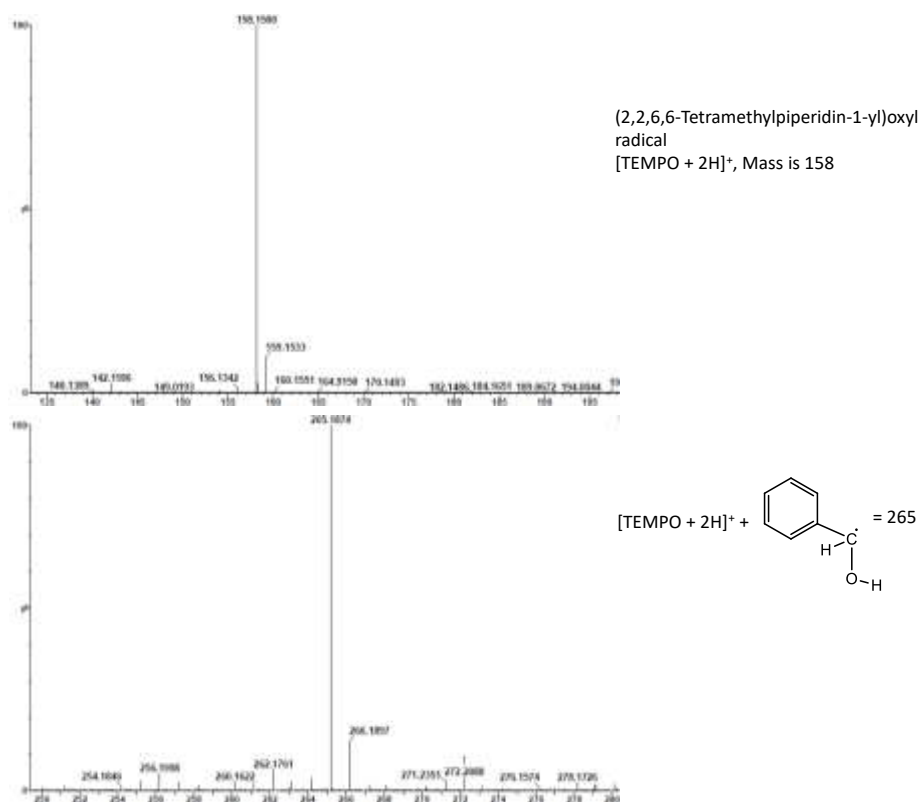


Fig. S15: TEMPO was introduced into the reaction mixture for BA oxidation by PE-CQDs. HRMS spectra were recorded before the start of the experiment and after irradiation with light for 2 h. Only [TEMPO+2H]⁺ was observed at the beginning due to the acidic PE-CQD solution. (a) while TEMPO formed an adduct with the carbon radical species after irradiation with light (b).

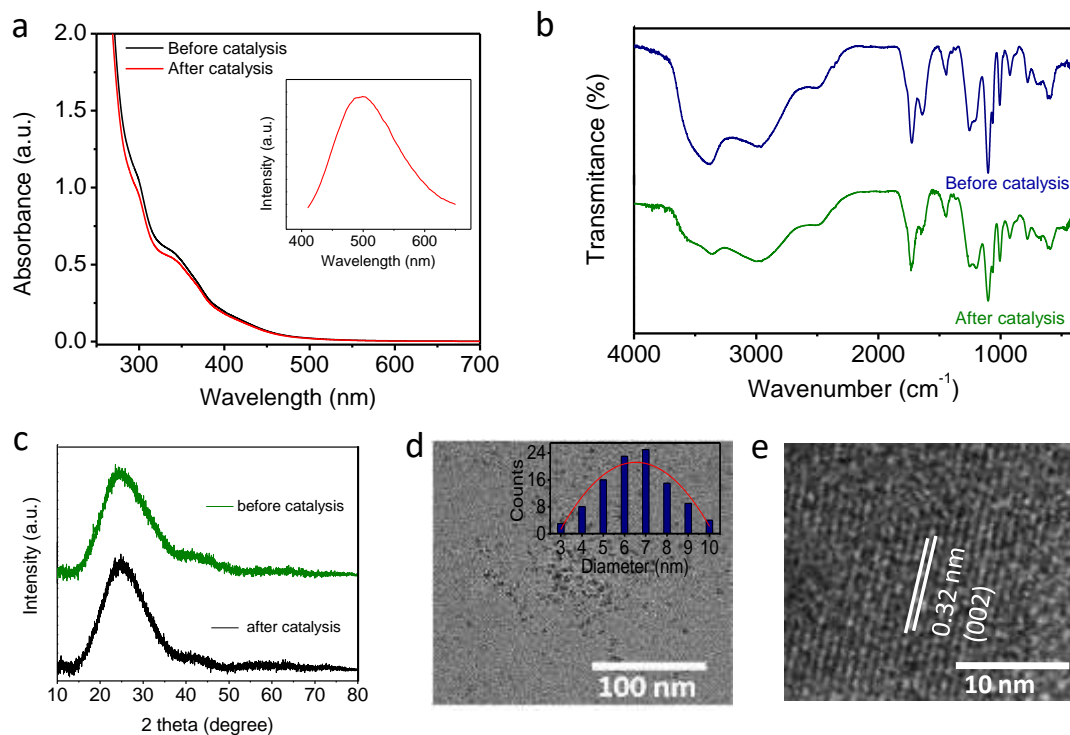


Fig. S16. a, UV–Visible absorption spectra of PE-CQDs before and after the catalysis. Inset in b is photoluminescence emission spectrum (excitation wavelength 390 nm) of PE-CQDs after catalysis and **b**, FT-IR spectra of PE-CQDs before and after the catalysis. **c**, PXRD pattern of fresh and used PE-CQDs. **d**, A low magnification TEM image of the used PE-CQDs (inset is the particle size distribution) **e**, HR-TEM image of an used PE-CQD.

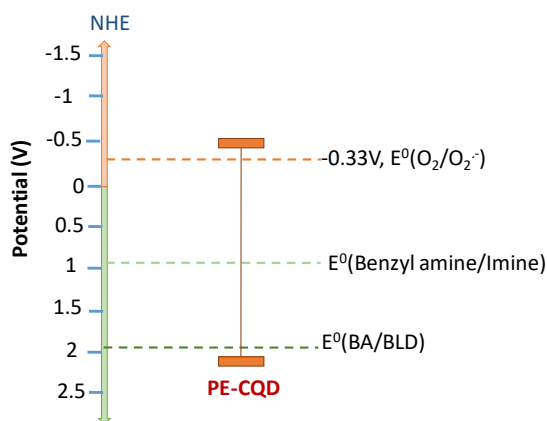


Fig. S17: Possible band positions of PE-CQDs.

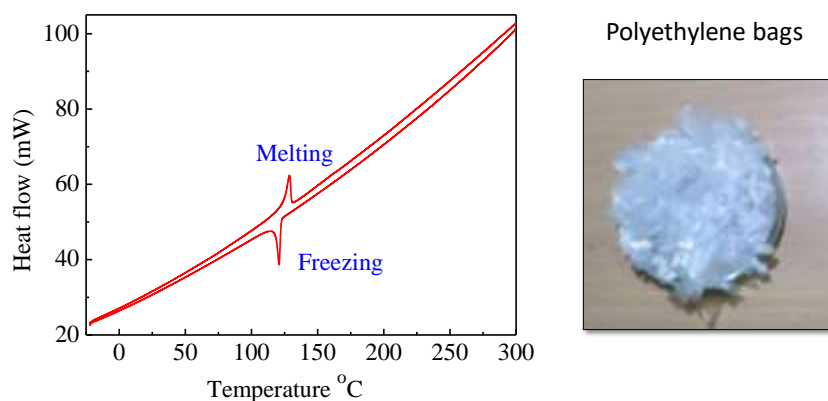


Fig. S18: DSC curve of polyethylene used for PE-CQDs synthesis. A photograph of the cut pieces of a PE bag is also shown on the right side.

Differential scanning calorimetric characterization of commercial polyethylene: In order to ascertain that waste polyethylene can also be converted to CQDs, we have used commercial polyethylene bags as starting material. Polyethylene are classified in two categories, i) low density polyethylene (LDPE, density: 0.922-0.934 g/cm³) and ii) high density polyethylene (HDPE, density: 0.935-0.96 g/cm³) which exhibit characteristic melting and freezing point. The melting temperature of commercial PE bags used here was estimated to be 127.5 °C, indicates that these are HDPE.

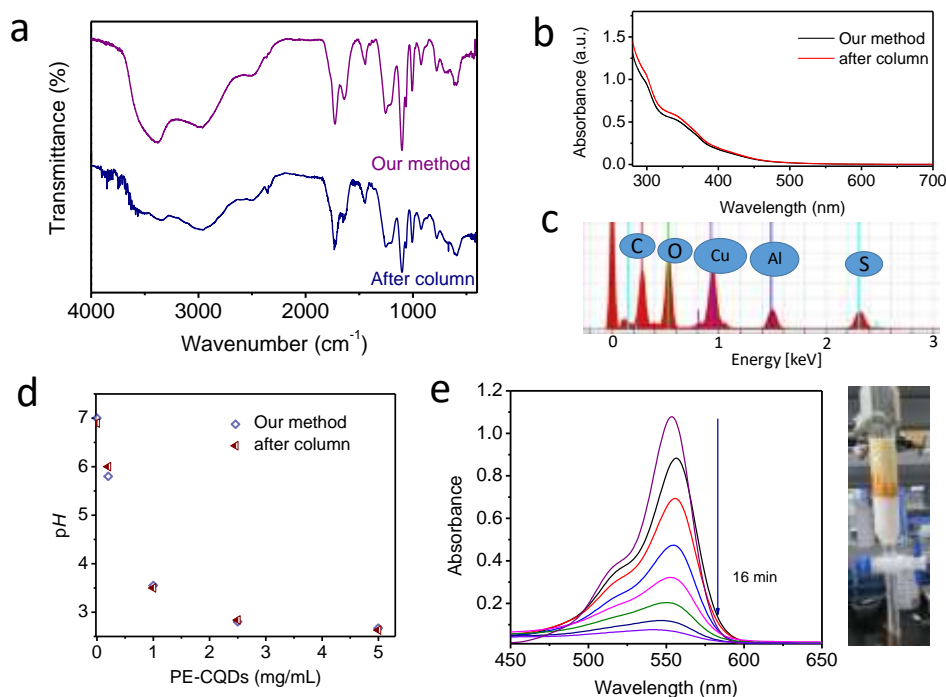


Fig. S19. a, FT-IR spectra and b, UV-Visible absorption spectra of PE-CQDs before and after the column separation. c, TEM-EDS spectrum of PE-CQDs obtained after column separation. d, pH of the PE-CQDs before and after column separation at different concentration. e, UV-visible absorption spectra of Rh-B at different time interval during catalytic degradation using PE-CQDs obtained by column separation (photographic image of the column shown on the right side).

Table S1: To optimise the formation of PE-CQDs, we have carried out the reactions at different sulphuric acid concentrations. It was observed that C-dot formation starts at 7M H₂SO₄ though the yield was very less. The yield increases with the H₂SO₄ concentration (images given on the right of the table show the gradual increase of carbon dots yield).







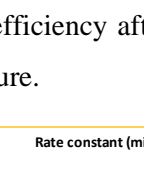
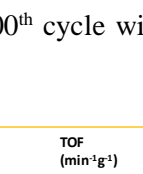
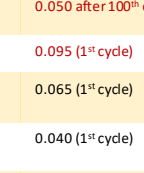
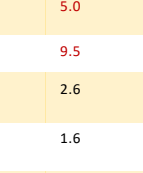
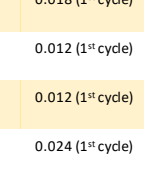
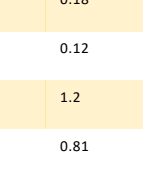
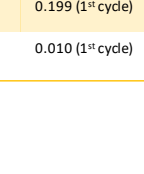
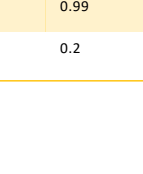
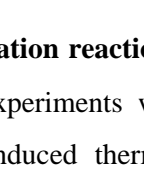
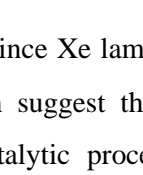
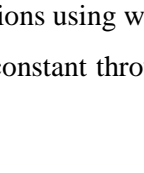
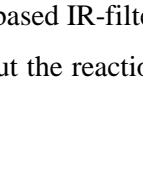
H ₂ SO ₄ Conc. (M)	Observation	Reaction aliquot	Unreacted PE
1M	CQDs do not form		
3M	CQDs do not form		
5M	CQDs do not form		
7M	Formation of CQDs begins		
9M	Partial PE conversion with CQD formation		
11M	Partial PE conversion with CQD formation		
13M	Partial PE conversion with CQD formation		
15M	Near complete PE conversion with CQD formation		
18M	Complete PE conversion with CQD formation		

Table S2: Comparison of PE-CQDs RhB degradation efficiency after 100th cycle with that of fresh commercial P25-TiO₂ and those reported in recent literature.

Sr. No.	Material	Catalyst amount	Light source	Rate constant (min ⁻¹)	TOF (min ⁻¹ g ⁻¹)	Ref.
1.	PE-CQDs after 100 th cycle	10 mg	Sunlight	0.050 after 100 th cycle	5.0	Our work
2.	P25-TiO ₂	10 mg	Sunlight	0.095 (1 st cycle)	9.5	Our work
3.	TiO ₂ nanocrystals	25 mg	1000 W, Xe-arc lamp	0.065 (1 st cycle)	2.6	2
4.	Ag/AgFeO ₂ nanocatalyst	25 mg	300W, Dy-lamp	0.040 (1 st cycle)	1.6	3
5.	g-C ₃ N ₄ /CuCr ₂ O ₄	100 mg	50W LED lamp	0.018 (1 st cycle)	0.18	4
6.	plasmonic ZnO/Ag/Ag ₂ WO ₄	100 mg	50W LED lamp	0.012 (1 st cycle)	0.12	5
7.	Fe ₃ O ₄ @TiO ₂ -C-dot	10 mg	Hg-vapour lamp	0.012 (1 st cycle)	1.2	6
8.	g-C ₃ N ₄	30 mg	500W, Xe-lamp	0.024 (1 st cycle)	0.81	7
9.	B-Doped g-C ₃ N ₄	200 mg	300W, Xe-lamp	0.199 (1 st cycle)	0.99	8
10.	S, N co-doped GQDs/TiO ₂	50 mg	300W, Xe-lamp	0.010 (1 st cycle)	0.2	9

Table S3 and S4: IR radiation effect on the BA oxidation reaction: Since Xe lamp and sun light contain IR radiation, we performed the following experiments which suggest that the reaction involves a photocatalytic process and not a photo-induced thermocatalytic process. First as a preliminary check, we have carried out all catalysis reactions using water-based IR-filter. The reaction temperature was constantly monitored and found to be constant throughout the reaction period (~33-

35°C) (Table S3). Second, we have also carried out the reaction in absence of light, but no conversion was noticed, confirming that the process is not purely thermocatalytic and irradiation by visible light is mandatory.

Table S3: Temperature of the reaction medium throughout the reaction period.

Reaction time	0 h	1 h	2 h	3 h	4 h
Temperature (°C)	33	34	33	33	35

To prove that this reaction is actually not a photo-induced thermocatalytic process we have carried out the reaction using light having 400-500 nm wavelength range by using a 3-LED setup (Newport, USA). The reactants indeed showed conversion to products, given in Table S4 inferring that the reaction is photocatalytic in nature.

Table S4: Conversion efficiency in different light source.

Reaction condition	Time (hour)	Conversion (%)
Xe-lamp with water circulation	4	68%
Reaction in dark	4	<1%
400-500 nm	4	17%

Table S5: Comparison of BA oxidation activity reported in this study with that of other efficient heterogeneous catalysts.

(**Note:** For the purpose of comparison, the most efficient catalysts from the recent literature were selected. However, such a comparison is not straightforward since experimental conditions vary in different studies. Therefore, the important reaction parameters such as amount of the catalyst and reactant, solvent, reaction atmosphere, time and temperature etc. are included in the table. Entries 2,3 and 4 demonstrates the effect of oxygen atmosphere.).

(r.t.: Room temperature. Conv.: Conversion, Select: Selectivity, BTF: Benzotrifluoride)

Sr. No.	Catalyst	Catalyst Amount	Amount of BA (mmol)	Time (h)	Temp. ($^{\circ}$ C)	O ₂ /Air	Solvent	Conv. (%)	Select. (%)	Ref.
1.	Carbon dots	25 mg	0.5	4	r.t	Air	CH ₃ CN	68	>90	Our work
2.	mpg-C ₃ N ₄	50 mg	0.65	3	100	O ₂	Trifluorotoluene	57	>99	10
						Air		11	>99	
3.	Ni-TiO ₂	80 mg	0.5	1	r.t	O ₂	BTF	86	99	11
						Air		6	99	
4.	Au ₉ -Pd ₁ /LDH	24 mg	0.1	5	r.t	O ₂	BTF	91	>99	12
						Air		27	>99	
5.	TiO ₂ @CdS	8 mg	-	2	r.t	O ₂	BTF	55	95	13
6.	Ir/TiO ₂	300 mg	300	6	60	-	Solvent free	8.9	92	14
7.	Porous BiOCl	50 mg	0.05	8	r.t	-	Toluene	70	-	15
8.	BiOCl-Au	50 mg	0.5	8	r.t	O ₂	CH ₃ CN	75	>99	16
9.	Dye -TiO ₂	8 mg & TEMPO	0.1	18	r.t	O ₂	BTF	80	98	17
10.	CdS-SnO ₂	50 mg	2	8	r.t	O ₂	CH ₃ CN	82	96	18
11.	Bi ₄ O ₅ Br ₂	200 mg	0.025	8	r.t	O ₂	CH ₃ CN	90	>99	19
12.	CsPbBr ₃ /P-25	25 mg	0.0005	20	80	O ₂	Toluene	50	>99	20
13.	TiO ₂ @NH ₂ -(Ti) MOF	50 mg	0.3	10.5	r.t	O ₂	BTF	37	-	21
14.	CN _x -Ni	5 mg	0.03	24	r.t	-	Phosphate buffer	72	99	22
15.	AuPd-TiO ₂	20 mg	0.04	5	r.t	O ₂	Toluene	87	>99	23

Note S1: Calculation of Apparent Quantum Efficiency (AQE): In order to calculate the AQE for the photocatalytic BA oxidation, we considered the reaction in direct sunlight with a reaction yield of 67% in 4 h and the solar spectrum at the sea-level (Fig. S11a). Our sun-light intensity may slightly vary and therefore the calculated efficiencies can be considered representative, with a minimal deviation from expected values. An additional complicacy arises because the estimated AQE can be further increased by using larger amount of PE-CQDs or benzyl alcohol or by considering conversion in the first few minutes only (the reaction becomes slow progressively as BA gets consumed). For calculation of overall efficiency, we counted the number of incident photons from higher energies till 500 nm where, based on the UV-Vis absorption spectrum of PE-CQDs, the absorption is >95%. For calculations of efficiencies in the 300-400 nm, 400-500 nm, 500-600 nm and 600-700 nm, the photon numbers in the respective regions were calculated separately and yields were estimated using diode assemblies (Newport, USA) mimicking solar spectrum. The apparent quantum efficiency we report below, in all probability, is smaller than the actual quantum efficiency because the number of absorbed photons is expected to be lesser than that of incident ones.²⁴The incident power on the sample can be represented as:

$$P_{\text{incident}} = \rho_{\text{incident}}(\lambda) \times A_{\text{sample}}$$

A_{sample} is the area exposed to incident light (12 cm²), $\rho_{\text{incident}}(\lambda)$ is the incident power on the sample corresponding to photon of wavelength λ .

The incident powers on the sample was estimated to be 168, 35 and 133 mW in the wavelength range of 300-500 nm, 300-400 nm, 400-500 nm (considering >95% photon absorption by PE-CQDs), and 155 and 144 mW in 500-600 nm and 600-700 nm (considering remaining <5% absorption) respectively. The number of incident photons per second, as a function of wavelength can be expressed as:

$$N_{ph}(\lambda) = \frac{\rho_{\text{incident}}(\lambda)}{E_{ph}(\lambda)}$$

Where $E_{ph}(\lambda) = hc/\lambda$ is the photon energy for the corresponding wavelength. For example, the total number of photons incident on the sample per second within wavelength range of 400-500 nm can be calculated as:

$$N_{ph,incident}(400 - 500) = \int_{400}^{500} \frac{\rho_{\text{incident}}(\lambda) \times \lambda}{hc} d\lambda$$

The AQE can be derived from the following equation:

$$AQE = n (\text{No. of electron or hole}) \times \frac{\text{Number of benzaldehyde molecule produced}}{\text{Number of incident photons}} \times 100 (\%)$$

For benzyl alcohol oxidation n is 2.

(For 400-500 nm):

$$AQE = 2 \times \frac{0.0000425}{0.00182} \times 100(\%)$$
$$= 2.3 \%$$

Similarly for 300-400, 500-600, 600-700 nm ranges, the calculated AQE are 4.8, 0.48 and 0.026% respectively (Fig. S11b). Overall AQE <500 nm where light absorption of PE-CQDs is >95% = 7.7%.

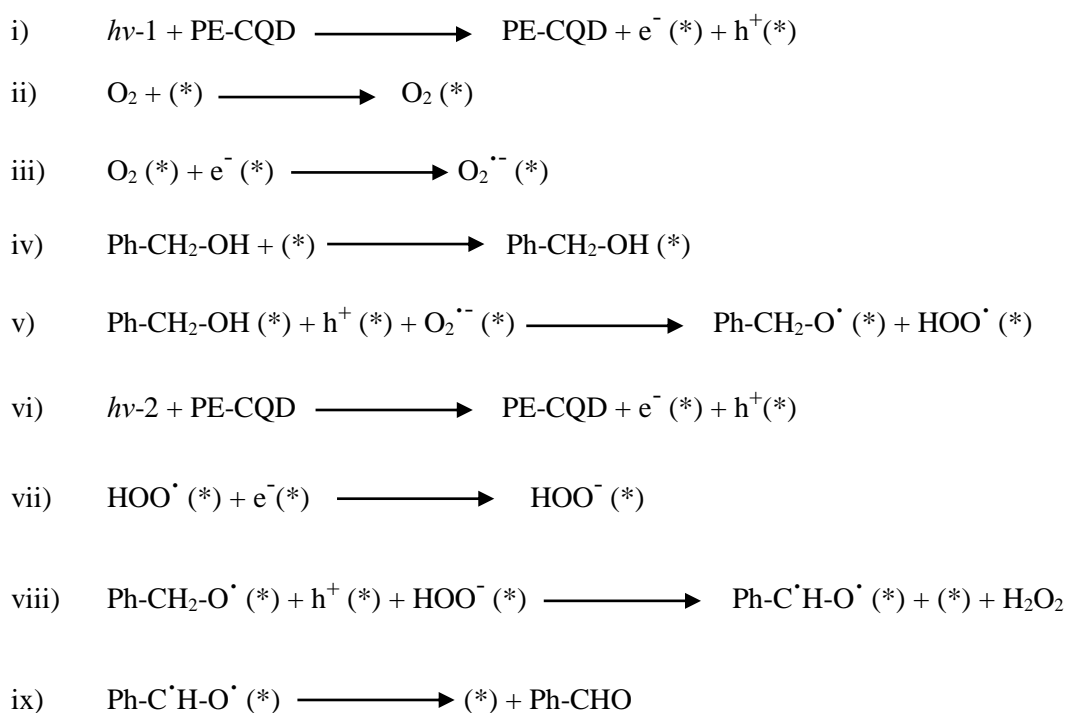
Note S2: Probable benzyl alcohol photo-oxidation reaction mechanism: As described in the main text, the BA oxidation experiments in the oxygen saturated and oxygen depleted solvents have established that the molecular oxygen acts as a reactant in the process. Further elucidation of the reaction mechanism showed that both photo-generated electrons and holes are responsible for the reaction. Since this reaction is known to be mediated by radicals generated by transfer of electrons and holes, we have carried out a series of controlled experiments using radical scavengers. Two types each (total four) of radical scavengers were used.¹⁰ Two scavengers were used either to scavenge the photogenerated electrons or the radical species generated by its transfer respectively. Similarly, two other scavengers were used to neutralize either the photogenerated holes or the corresponding radical. In each case, four equivalents of scavengers for each BA molecule were used and both scavengers in each set of experiments led to the same conclusions (Fig. 5c in the manuscript).

Since O₂ alone could not oxidize BA in reasonable amounts, O₂ activation by electrons is therefore vital. The activated O₂ responsible for BA oxidation was found to be superoxide radicals (O₂^{•-}), as the addition of benzoquinone as superoxide radicals scavenger suppressed the conversion (30% yield after 4 h). We further assumed that if we carry out the oxidation reaction in presence of increasing amount benzoquinone, more of O₂^{•-} will be lost and the reaction will be progressively slower. We indeed found the same when we increased the amount of benzoquinone (1, 2, 10 and 20 mmole) in the reaction mixture, conversion efficiency decreased systematically (~50%, ~40%, ~32% and ~30% respectively, see the Fig. S13a). Another controlled experiment was performed using another superoxide anion radical i.e, ascorbic acid. A similar phenomenon was also observed as previous experiment (25-28% yield after 4h, see Fig. S13b). We have then carried out electron trapping experiment using silver nitrate and percentage of conversion was found to be 29% after 4 h. These two similar reaction rates suggest that both the electron transfer to molecular O₂ and O₂^{•-} attack on BA are contributed comparably to the reaction rate.

It has been previously established that the transfer of photogenerated holes to the BA molecules results in formation of a carbon centered radical. Using sodium sulfate as hole scavenger, the conversion was suppressed to a similar extent (8% yield after 4 hr). Further, we have performed a reaction in presence of butylatedhydroxytoluene as its scavenger. The BA conversion was suppressed to ~7% after 4 h suggesting that oxidation reaction indeed goes via formation of carbon radical species. We confirmed the generation of this radical by a trapping experiment using TEMPO ((2,2,6,6-Tetramethylpiperidin-1-yl)oxyl radical) and detecting the trapped radical by high-resolution mass-spectroscopy (HRMS, Fig.S13).²⁵

Generation of H₂O₂ in the reaction mixture was also detected colorimetrically by KMnO₄ titration.²⁶ Overall, two photons are used to oxidize one BA molecule to benzaldehyde and simultaneously reduce one oxygen molecule to H₂O₂.

Based on these findings and previous literature,¹⁶ a reaction scheme is proposed (Scheme 1) in the main manuscript. The corresponding elementary steps are as follows:



Note S3: Positions of valence and conduction bands of PE-CQDs: We suggest the conduction and valence band positions based on band-gap of PE-CQDs (from UV-Vis absorption measurement) and other literature reports. The reduction potential for the O₂ to superoxide anion radical is -0.33 V (vs. NHE) and the oxidation potential of benzyl alcohol (BA) to benzaldehyde has been estimated to be 1.98 V (vs. NHE),²⁷ the two potentials being 2.31 V apart. In order for molecular oxygen to oxidize BA photocatalytically in presence of PE-CQDs, the valence band position of PE-CQD has to be more positive than 1.98 V and the conduction band position more negative than -0.33V. The band-gap of

PE-CQD was found to be 2.59 eV which is sufficient to straddle both these reaction potentials. Since our experiments confirm both BA oxidation and O₂ reduction, the band positions for PE-CQDs may be proposed as follows with an accuracy of ± 0.28 eV (For comparison, we also include the same for TiO₂,^{27,28} whose catalytic efficiency is compared with PE-CQDs.), Supplementary Fig. 15.

References

- 1 S. Rasalingam, C.-M. Wu and R. T. Koodali, *ACS Appl. Mater. Interfaces*, 2015, 7, 4368–4380.
- 2 D. Tang and G. Zhang, *Ultrason. Sonochem.*, 2017, 37, 208–215.
- 3 A. Akhundi and A. Habibi-Yangjeh, *J. Colloid Interface Sci.*, 2017, 504, 697–710.
- 4 M. Pirhashemi and A. Habibi-Yangjeh, *J. Colloid Interface Sci.*, 2017, 491, 216–229.
- 5 R. K. Das, J. P. Kar and S. Mohapatra, *Ind. Eng. Chem. Res.*, 2016, 55, 5902–5910.
- 6 Z. Tong, D. Yang, Z. Li, Y. Nan, F. Ding, Y. Shen and Z. Jiang, *ACS Nano*, 2017, 11, 1103–1112.
- 7 S. C. Yan, Z. S. Li and Z. G. Zou, *Langmuir*, 2010, 26, 3894–3901.
- 8 D. Qu, M. Zheng, P. Du, Y. Zhou, L. Zhang, D. Li, H. Tan, Z. Zhao, Z. Xie and Z. Sun, *Nanoscale*, 2013, 5, 12272–12277.
- 9 H. Fujito, H. Kunioku, D. Kato, H. Suzuki, M. Higashi, H. Kageyama and R. Abe, *J. Am. Chem. Soc.*, 2016, 138, 2082–2085.
- 10 F. Su, S. C. Mathew, G. Lipner, X. Fu, M. Antonietti, S. Blechert and X. Wang, *J. Am. Chem. Soc.*, 2010, 132, 16299–16301.
- 11 H. She, H. Zhou, L. Li, L. Wang, J. Huang and Q. Wang, *ACS Sustain. Chem. Eng.*, 2018, 6, 11939–11948.
- 12 Z. Wang, Y. Song, J. Zou, L. Li, Y. Yu and L. Wu, *Catal. Sci. Technol.*, 2018, 8, 268–275.
- 13 Z. Chen and Y. J. Xu, *ACS Appl. Mater. Interfaces*, 2013, 5, 13353–13363
- 14 W. Feng, G. Wu, L. Li and N. Guan, *Green Chem.*, 2011, 13, 3265–3272.
- 15 H. Li, F. Qin, Z. Yang, X. Cui, J. Wang, L. Zhang, *J. Am. Chem. Soc.*, 2017, 139, 3513–3521
- 16 L. Ding, H. Chen, Q. Wang, T. Zhou, Q. Jiang, Y. Yuan, J. Li and J. Hu, *Chem. Commun.*, 2016, 52, 994–997.
- 17 M. Zhang, C. Chen, W. Ma and J. Zhao, *Angew. Chemie*, 2008, 120, 9876–9879.
- 18 Y. Liu, P. Zhang, B. Tian and J. Zhang, *ACS Appl. Mater. Interfaces*, 2015, 7, 13849–13858
- 19 C. Zheng, G. He, X. Xiao, M. Lu, H. Zhong, X. Zuo and J. Nan, *Appl. Catal. B Environ.*, 2017, 205, 201–210.
- 20 S. Schünemann, M. van Gastel and H. Tüysüz, *ChemSusChem*, 2018, 11, 1, 2057–2061.

- 21 X. Li, Y. Pi, Q. Hou, H. Yu, Z. Li, Y. Li and J. Xiao, *Chem. Commun.*, 2018, 54, 1917–1920.
- 22 H. Kasap, C. A. Caputo, B. C. M. Martindale, R. Godin, V. W. Lau, B. V Lotsch, J. R. Durrant and E. Reisner, *J. Am. Chem. Soc.*, 2016, 138, 9183–9192.
- 23 T. Jiang, C. Jia, L. Zhang, S. He, Y. Sang, H. Li, Y. Li, X. Xu and H. Liu, *Nanoscale*, 2015, 7, 209–217.
- 24 Kibria, M.G.; Chowdhury, F.A.; Zhao, S.; AlOtaibi, B.; Trudeau, M. L.; Guo, H.; Mi, Z., *Nat. Commun.* 2015, 6, 1-8.
- 25 Marjasvaara, A.; Torvinen, M.; Vainiotalo, P., *J. Mass Spectrom.* 2004, 39, 1139–1146.
- 26 Chen, H.; Liu, C.; Wang, M.; Zhang, C.; Luo, N.; Wang, Y.; Abroshan, H.; Li, G., *ACS Catal.*, 2017, 7, 3632–3638.
- 27 X. Xiao, J. Jiang, L. Zhang, *Applied Catalysis B: Environmental*, 2013, 142, 487-493.
- 28 T. Chen, G. Liu, F. Jin, M. Wei, J. Feng, Y. Ma., *Phys. Chem. Chem. Phys.*, 2018, 20, 12785.